

Nucleation of Solids in Solids: Ferrites and Martensites

Madan Rao¹ and Surajit Sengupta²¹Raman Research Institute, C.V. Raman Avenue, Bangalore 560080, India²S. N. Bose National Centre for Basic Sciences, Block JD, Sector III, Salt Lake, Calcutta 700091, India
(Received 28 September 2001; revised manuscript received 21 April 2003; published 23 July 2003)

When a solid such as iron is cooled across a structural transition, its final microstructure depends sensitively on the cooling rate and the depth of quench. For instance, an infinitesimally slow cooling or a shallow quench results in an equilibrium “ferrite,” while a rapid cooling or a deep quench gives rise to a metastable twinned “martensite.” In this paper, we arrive at a single formalism which qualitatively describes the transformation to *both* a ferrite and a martensite. Fundamental to this understanding is our identification of the crucial dynamical role played by *nonelastic* degrees of freedom in determining the final microstructure of the product solid.

DOI: 10.1103/PhysRevLett.91.045502

PACS numbers: 81.30.Kf, 63.70.+h, 64.60.Qb, 64.70.Kb

What determines the microstructure of a solid as it is cooled across a structural transition? To our knowledge, there exists no theoretical framework for the dynamics of solid-state transformations which can, even in principle, discuss the conditions under which the various microstructures obtain. Here we focus on a specific but ubiquitous class of microstructures called *martensites* and *ferrites*. Martensites [1] are long-lived metastable twinned products obtained when a solid such as iron is either rapidly quenched or subject to a deep quench across a structural transition. In contrast, any parent solid cooled ever so slowly or subject to a shallow quench across a structural transition will always give rise to an equilibrium crystalline product (generically called ferrite). In this Letter we develop a dynamical framework addressing the conditions under which the “uniform” ferrite and “twinned” martensite obtain.

To develop this unified framework, we will need to go beyond the conventional description of martensite dynamics, written solely in terms of elastic strain [2]. We provide evidence from simulations done on a model solid, for the crucial role played by nonelastic variables, such as density fluctuations, in determining the dynamics of nucleation and its final microstructure. It is only with this “enlargement” of the dynamical variables that we may describe the formation of *both* martensite and ferrite [3], at least in this class of model solids.

An important outcome of our work is that the selection of the final microstructure, e.g., ferrite or martensite, is dictated by dynamics and not by energetics alone. Such dynamical criteria for the selection of the final product have been suggested by other authors (e.g., Ref. [4]).

Our strategy is to start from a microscopic description of solid-state nucleation using a molecular dynamics (MD) simulation and develop an appropriate continuum description by a coarse-graining procedure [5]. For conceptual clarity, we study a two dimensional (2D) model system [6] which exhibits exactly two distinct equilibrium solid phases—square and triangular (rhombic unit cell) using an MD simulation on particles (“atoms”)

interacting with an *effective* potential. Though the issues discussed here go beyond this simple 2D model, our work may be directly applicable to 2D transformations such as in In-Tl or $\text{YBa}_2\text{Cu}_3\text{O}_7$ [2], solids in confined geometries [7,8], and solid films on surfaces or solid wetting layers [9].

MD simulations of a model solid.—The system consists of N particles ($N = 2500, 12\,100$) interacting via an effective (purely repulsive) potential, the sum of a 2 body $V_2(r_{ij}) = v_2(\sigma/r_{ij})^{12}$ and a short range 3 body $V_3(\mathbf{r}_i, \mathbf{r}_j, \mathbf{r}_k) = v_3[\sin^2(4\theta_{ijk}) + \sin^2(4\theta_{jki}) + \sin^2(4\theta_{kij})]$ in a 2D box of “volume” V with periodic boundary conditions [6]. Particles i and j are separated by a distance r_{ij} and θ_{ijk} is the bond angle at j between r_{ij} and r_{jk} . The units of length and energy are set by σ and v_2 , respectively, making the unit of time $\sigma\sqrt{m/v_2}$, where m is the particle mass. Using typical values, an MD time step of 0.001 corresponds to a real time of around 1 fs. We use a constant NVT -strain ensemble, where the temperature T is maintained by a Nosé-Hoover thermostat [10]. V_2 favors a triangular lattice ground state while V_3 is minimized when $\theta_{ijk} = 0, \pi/4, \pi/2$ favoring a square lattice. The order parameter $\langle \Omega \rangle = N^{-1} \sum_i \Omega_i = N^{-1} \sum_i \langle \Omega_0 \rangle^{-1} \sum_{jk} \langle \sin^2(4\theta_{ijk}) \rangle$ has been constructed to take values 0 (1) in a perfect square (triangular) lattice, angular brackets denote ensemble averages. The phase diagram [6] is obtained by equilibrating the system at various values of T and v_3 for different densities (Fig. 1).

Starting from the equilibrium square phase, we may transform into the triangular phase by either changing T or v_3 . While the typical quench schedule is a cut through the T - v_3 plane, we find it more convenient to change v_3 while holding the temperature T fixed. This transformation protocol allows for a more transparent interpretation of the MD results. We have found that the essential physics is unaltered by this constant T transformation; in addition it allows us to write the coarse-grained dynamics in terms of the usual Helmholtz free-energy functional. Experimentally, this may be achieved in bulk materials by changing external fields, such as pressure or electric

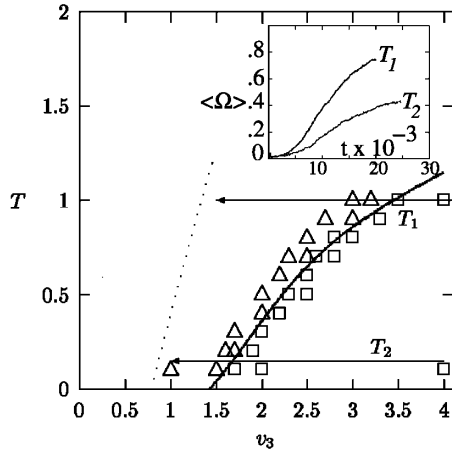


FIG. 1. Equilibrium phase diagram for $N = 2499$ at $\langle \rho \rangle = 1.05$, showing the square (\square) and triangle (\triangle) phases separated by a phase boundary (dark line). Arrows T_1 and T_2 are the constant temperature transformation protocols into the region where square is metastable (bounded by dotted line [6]). Inset: $\langle \Omega \rangle$ versus t for the two transformation protocols.

field, which couple to the faster electronic degrees of freedom thereby affecting potentials such as v_3 ; in colloidal crystals held between glass plates, the crystal structure may be manipulated by external modulating potentials produced by crossed laser beams [7].

Figure 1 shows two representative transformation protocols [high (T_1) and low (T_2)] starting from the equilibrium square into the region where the square phase is metastable. Following either protocol, the product phase is formed by a process of nucleation and growth [Fig. 1 (inset)], but while the T_1 nucleation is homogeneous, the T_2 nucleation needs to be seeded by defects (heterogeneous), e.g., by a single vacancy.

We define coarse-grained dynamical variables via instantaneous displacements \mathbf{u} of the particles from the ideal square lattice—the nonlinear elastic strain ϵ_{ij} , density fluctuations about the mean $\langle \rho \rangle$, $\phi = (\rho - \langle \rho \rangle)/\langle \rho \rangle$ (referred to as vacancy/interstitial or simply VI density [11]), and dislocation density (density of 5–7 disclination pairs).

Our simulations show that nucleation of a triangular region within the square initially produces density fluctuations (VIs) at the interface which relax with a bare diffusion coefficient D_v , which in general may be anisotropic and different from its value $D(v_3, T)$ at equilibrium [the latter shows Arrhenius behavior, $\propto \exp[-A(v_3)/k_B T]$, with an activation $A(v_3) \approx 1.4$]. An MD snapshot following the T_1 protocol [Fig. 2(a)] shows the growth of an “isotropic” nucleus (after averaging over initial conditions and a space-time window). Inset shows x - y trajectories of five particles for $5 \times 10^3 < t < 25 \times 10^3$, chosen to lie along a row (x axis) at $t = 0$. At these times the particles are part of the growing nucleus, and their trajectories reveal significant diffusive motion. The bare VI diffusion coefficient D_v is isotropic and roughly equal to its equilibrium value $D(v_3, T)$. This allows

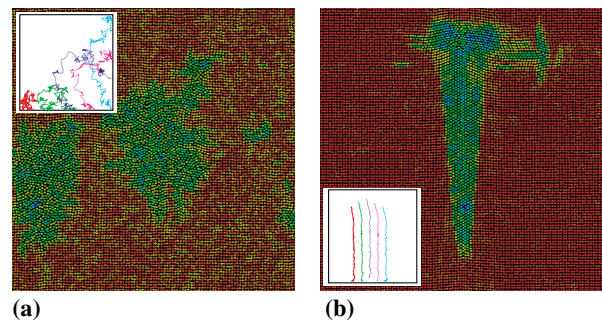


FIG. 2 (color online). MD snapshot of a 110^2 system (a) *isotropic ferrite* nucleus at $t = 10^4$ (inset: trajectories of five chosen particles). (b) *Anisotropic twinned* nucleus at $t = 6 \times 10^3$ (inset: trajectories of five chosen particles which move from bottom to top). Colors (gray scale) code the local order parameter $\langle \Omega_i \rangle$ going from red (dark) — \square to blue (light) — \triangle .

the VIs to diffuse fast and annihilate each other, thus encouraging the triangular phase to grow isotropically [Fig. 2(a)]. The time averaged VI density ϕ rapidly relaxes to 0. Since there is a chemical potential gain in forming the triangular nucleus, the nucleus size R grows linearly with time t , as observed in our simulation. The critical nucleus is untwinned and grows to form a polycrystalline triangular solid; subsequently grain boundaries reorient to form a homogeneous triangular phase (“ferrite”).

In contrast, an MD snapshot following the T_2 protocol [Fig. 2(b)], shows the growth of a “needlelike” nucleus. Recall that the T_2 protocol needed a vacancy seed to initiate nucleation. At these low temperatures the seed vacancy does not diffuse away [the bare VI diffusion D_v is spatially anisotropic with a value much smaller than its equilibrium value $D(v_3, T)$]; dominant density fluctuations correspond to a coordinated movement of a line segment of atoms along the square axes. Once these fluctuations get large enough, they grow into a critical nucleus which is highly anisotropic, breaking the C_4 symmetry dynamically. The shear strain profile ϵ_{xy} [Fig. 3 (inset)] integrated over y changes sign across an interface which sharpens with the march of time. The critical nucleus is therefore twinned with the twin interface along one of the square axes [12]. Figure 3 shows the time development of the VI profile ϕ integrated over x as a function of y (along the twin interface). The VIs while staying separated from each other are found concentrated at the interface of the growing nucleus. We now follow individual particle trajectories as the growing nucleus invades the surrounding square territory. Figure 2(b) (inset) shows trajectories for $10^3 < t < 16.5 \times 10^3$ of five particles chosen to lie along a row (x axis) at $t = 0$. At these times the particles are part of the growing nucleus, and their trajectories reveal highly correlated (“military”) motion characteristic of martensites. If instead, the particles are chosen to lie along a twin column (y axis), then apart from thermal fluctuations, the particle positions change only when they encounter the moving

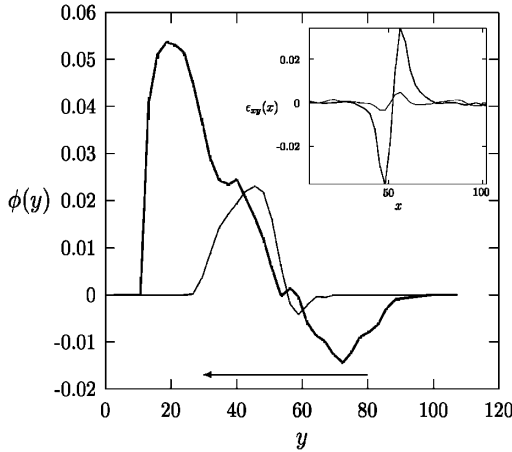


FIG. 3. Profile of ϕ at $t = t_1(2000)$ and $t_2(5000)$. Arrow shows the direction of particle displacements resulting in increased density at one end of the nucleus and reduced density at the other. Inset: profile of ϵ_{xy} at the two times.

front. We determine that the transformation front moves with a constant velocity, $v_f = 9.7$, which compares well with the longitudinal sound velocity calculated from the bulk modulus in the square phase. In the direction transverse to the twin interface, the nucleus grows by step (coherence dislocation) formation [Fig. 2(b)].

Continuum Landau theory.—The MD simulation highlights the dynamical role played by (nonelastic) density fluctuations ϕ in determining the mode of nucleation and the nature of the critical nucleus. In developing a continuum theory of solid-state nucleation that describes both ferrite and martensite we shall take only two key inputs from our MD simulation—(i) the relevant dynamical variables should include *both* strain ϵ_{ij} and density fluctuations ϕ , and (ii) the bare diffusion coefficient of the density fluctuations is strongly temperature dependent. The continuum description of the nucleation dynamics requires a free-energy functional $F[\epsilon_{ij}, \phi]$; the form of the strain-only part may be obtained from our 2D-model system by a method of coarse graining [6], while the ϕ dependence may be constructed from symmetry arguments. For convenience, we work with the simplest dimensionless free-energy functional describing the first-order square ($\langle \epsilon_{xy} \rangle = 0$) to rhombus ($\langle \epsilon_{xy} \rangle = \pm e_0$) transition on tuning the parameter a (monotonic function of T) [2,6],

$$F = \int_x (\nabla w_{ij})^2 + a\epsilon_{xy}^2 + b\epsilon_{ii}^2 - \epsilon_{xy}^4 + \epsilon_{xy}^6 + \gamma\phi^2 + C\phi\epsilon_{ii}, \quad (1)$$

where $w_{ij} \equiv \partial_i u_j$ is the deformation tensor and C couples the density fluctuations to the longitudinal strain ϵ_{ii} ($= \text{Tr}\epsilon_{ij}$). Fixing a in the region where the square is metastable, we nucleate a small “droplet” of the rhombus, while simultaneously creating an envelope of ϕ around it; this is the initial condition for the dynamical equations in the displacements \mathbf{u} and ϕ [3,11]:

$$\partial_t \phi + \mathbf{v} \cdot \nabla \phi = D_v \nabla^2 (2\gamma\phi + C\epsilon_{ii}). \quad (2)$$

Though the bare mobility D_v may in general be anisotropic and strongly temperature dependent, we shall assume for simplicity, an isotropic albeit temperature dependent form. The velocity field $\mathbf{v} = \dot{\mathbf{u}} + \Gamma_u C \nabla \phi$, where Γ_u is the microscopic kinetic coefficient of \mathbf{u} .

Since at low a (high temperatures) D_v is large, we find that ϕ diffuses to its equilibrium much faster than the time for the critical nucleus to form. The critical nucleus is then a ferrite (which minimizes F in the absence of ϕ) with no twin interfaces. The free-energy gradient across the transformation front provides the driving force for the subsequent isotropic growth of the nucleus with a constant speed. The final configuration is an equilibrium triangular ferrite phase. These results are consistent with the MD simulation of the T_1 transformation protocol.

On the other hand at higher a (lower temperatures) D_v is exponentially smaller; the nature of the critical nucleus is determined by computing the “first-passage time” τ_n . *A priori* we do not know whether the critical nucleus is twinned or not, and so we perform a variational calculation for both cases; the “true critical nucleus” is the one for which τ_n is smaller. It should be clear from the phenomenology just described that a naive extension of the standard nucleation theory valid for liquid-gas transitions [13], wherein the selection of the critical nucleus is determined entirely by relative free-energy barriers, would not yield the desired result; we need to solve the partial differential equations for the dynamical fields in order to estimate the nucleation time. This is in general not an easy task; happily the qualitative features may be obtained by an approximate calculation.

In the linearized equation for ϕ , the velocity field (ignoring lattice vibrations) reduces to the front velocity $\mathbf{v} = v_f \hat{\mathbf{n}} \delta[\mathbf{r} - \mathbf{R}(t)]$, where $\mathbf{R}(t)$ is the position of the moving interface and $\hat{\mathbf{n}}$ is the unit outward normal to the interface. Thus in the reference frame of the interface, the dynamics of ϕ is diffusive. Since the relaxation time to the local minima of F is much smaller than barrier hopping times, we may minimize the free energy with respect to the magnitude of ϵ_{ij} subject to boundary conditions appropriate to a growing nucleus and the constraint that ϕ takes its instantaneous value given by Eq. (2).

The calculation proceeds by recognizing that a perfect triangular solid is obtained from a perfect square by the deformation, $R'_i = (\delta_{ij} + \epsilon_{ij})R_j$, involving a shear $\epsilon_{xy} = \epsilon_{yx} = \epsilon$ and compression $\epsilon_{xx} = \epsilon_{yy} \approx \epsilon^2/2$. We therefore parametrize ϵ_{ij} by the single function $\epsilon(\mathbf{r}, t)$ [6]. This admits a variational ansatz for (i) ferrite: $\epsilon = 0$ outside a grain of size L and $\epsilon = e_0$ inside, connected by a linear interpolation with a given “interfacial thickness,” and (ii) twinned nucleus: $\epsilon = 0$ outside a rectangular grain of length L , width W , and $\epsilon = \pm e_0$ inside, connected by piecewise linear interpolations. The diffusion equation, $\partial_t \phi = D_v \nabla^2 (2\gamma\phi + C\epsilon_{ii})$ is solved with the initial

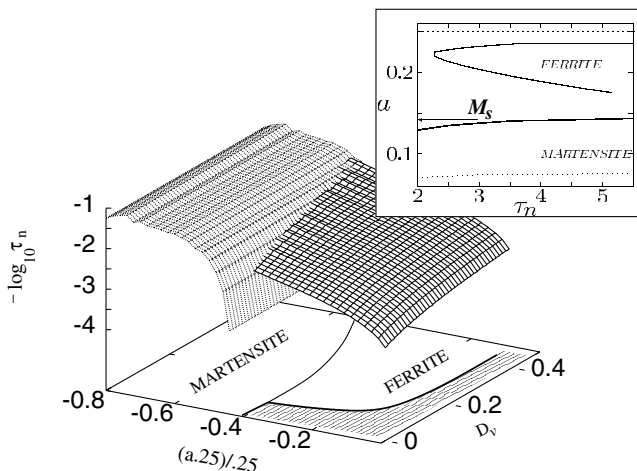


FIG. 4. First-passage time τ_n versus parameter a and diffusion coefficient D_v . Hatched area is the region in which solid transformation does not occur. The inset shows the cut across the 3D plot when $D_v = D_\infty \exp(-A/k_B T)$ ($D_\infty = 10^{14}$, $A = 7$, $\gamma = 0.2$ and $C = 0$). Upper dotted line is the equilibrium transition. At lower a , the single twin nucleates faster (bold line) than the ferrite (lower dotted line). Arrow (M_s) shows the value of a below which the twinned nucleus forms.

condition $\phi(\mathbf{r}, 0) = \Delta \mathbf{u} \cdot \hat{\mathbf{n}}$ ($\Delta \mathbf{u}$ is the geometrical mismatch at the square-triangle interface proportional to its length). Note that $\Delta \mathbf{u}$ is explicitly zero at the twin interface. The free energy of the grain at time t , $E(L, W, t)$, is obtained from Eq. (1), which we minimize with respect to the interfacial thickness for every L , W , and t . The barrier energy ΔE^* and size L^* , W^* of the critical nucleus at every time t is determined by the saddle point. The energy of the critical nucleus decreases with time, and so a crude but easily calculable estimate of the first-passage time is obtained (apart from unknown prefactors) by a self-consistent solution of the Kramers's formula $\tau_n = \Gamma^{-1} \exp[\Delta E^*(\tau_n)]$, where ΔE^* is the $\phi(\mathbf{r}, t)$ -dependent critical barrier energy. The accuracy of this self-consistent approximation and systematic corrections to this are analyzed in some detail in [14]. The results of this calculation are represented in a 3D plot (Fig. 4) which clearly shows that for low a (high temperatures), the true critical nucleus is a ferrite, while for large a (low temperatures) it forms a twinned bicrystal (martensite). Note that the martensite obtains in the regime where $D_v \approx 0$, implying that the martensitic transformation is *diffusionless*. In practice, of course, D_v and a are not independent; knowing the temperature dependence of D_v produces a cut in the D_v - a plane and describes the transformation curves of the solid. As an example (Fig. 4, inset), an Arrhenius form reproduces the well-known “0% isothermal transformation curves” [1]—the horizontal transformation curve beyond a sharp “martensite-start” temperature M_s independent of D_∞ and a ferrite nose. Note that, one needs to have a finite amount of undercooling even at $D = 0$ in order to obtain the

martensite. Also, by changing parameters such as the transformation temperature, we may entirely avoid the ferrite nose, indicating that for such systems the critical nucleus is always twinned. Admittedly this calculation is crude; however it does reproduce the qualitative features of martensitic nucleation. The most important outcome of this (and the MD) is that the *dynamics of the ϕ field determines the selection of the critical nucleus*.

In conclusion, we believe our work provides useful insights on the nucleation dynamics of ferrites and martensites. Fundamental to this understanding is our identification of the crucial dynamical role played by *nonelastic* degrees of freedom in determining the final microstructure of the product solid. We should however caution that these conclusions are based on an analysis of a model solid; similar results are obtained when the interparticle potentials are altered slightly. However in other kinds of solids, for instance where the energy cost for producing such density fluctuations is prohibitively large, some other mechanism for the selection of the final microstructure might be operative. A search for possible selection mechanisms in solid-state nucleation promises to be a challenging task for the future.

We thank the Isaac Newton Institute for Mathematical Sciences for support; M. R. thanks DST, India, for a Swarnajayanthi grant.

- [1] R. W. Cahn and P. Haasen, *Physical Metallurgy* (North-Holland, Amsterdam, 1996).
- [2] G. R. Barsch *et al.*, Phys. Rev. Lett. **59**, 1251 (1987); K. Ø. Rasmussen *et al.*, Phys. Rev. Lett. **87**, 055704 (2001); T. Lookman *et al.*, Phys. Rev. B **67**, 024114 (2003), and references therein.
- [3] M. Rao and S. Sengupta, Phys. Rev. Lett. **78**, 2168 (1997); Curr. Sci. **77**, 382 (1999); S. Sengupta and M. Rao, Physica (Amsterdam) **318A**, 251 (2003).
- [4] J. Bechhoefer *et al.*, Phys. Rev. Lett. **67**, 1266 (1991).
- [5] M. L. Falk and J. S. Langer, Phys. Rev. E **57**, 7192 (1998).
- [6] M. Rao and S. Sengupta, cond-mat/0106058.
- [7] *Ordering and Phase Transitions in Charged Colloids*, edited by A. K. Arora and B. V. R. Tata (VCH Publishers, New York, 1996).
- [8] C. Ghatak and K. G. Ayappa, Phys. Rev. E **64**, 051507 (2001).
- [9] L. Proville, Phys. Rev. Lett. **88**, 046102 (2002); J. Creuze *et al.*, Phys. Rev. Lett. **86**, 5735 (2001).
- [10] D. Frenkel and B. Smit, *Understanding Molecular Simulations* (Academic Press, San Diego, 1996).
- [11] P. C. Martin *et al.*, Phys. Rev. A **6**, 2401 (1972); P. M. Chaikin and T. C. Lubensky, *Principles of Condensed Matter Physics* (Cambridge University Press, London, 1995).
- [12] Note that our transformation involves a volume change and so admits a twinning pattern [2].
- [13] J. S. Langer, Ann. Phys. (N.Y.) **41**, 168 (1967).
- [14] J. Shillcock and U. Seifert, Phys. Rev. E **57**, 7301 (1998).